



## Quantifying the interaction of the C-terminal regions of polycystin-2 and polycystin-1 attached to a lipid bilayer by means of QCM

Daniela Behn<sup>a</sup>, Sabine Bosk<sup>a</sup>, Helen Hoffmeister<sup>b</sup>, Andreas Janshoff<sup>c</sup>, Ralph Witzgall<sup>b</sup>, Claudia Steinem<sup>a,\*</sup>

<sup>a</sup> Institut für Organische und Biomolekulare Chemie, Georg-August Universität, Tammannstr. 2, 37077 Göttingen, Germany

<sup>b</sup> Universität Regensburg, Universitätsstr. 31, 93053 Regensburg, Germany

<sup>c</sup> Institut für Physikalische Chemie, Georg-August Universität, Tammannstr. 6, 37077 Göttingen, Germany

### ARTICLE INFO

#### Article history:

Received 15 December 2009

Received in revised form 4 February 2010

Accepted 4 February 2010

Available online 11 February 2010

#### Keywords:

Autosomal dominant polycystic kidney disease

Quartz crystal microbalance

Membrane

Scaled particle theory

TRPP2

### ABSTRACT

The *pkd1* and *pkd2* genes encode for the proteins polycystin-1 (PC1) and polycystin-2 (PC2). These genes are mutated in patients diagnosed with autosomal dominant polycystic kidney disease. PC1 and PC2 interact via their C-terminal, cytosolic regions, which is an essential step in the regulation of cell proliferation and differentiation. Here, we developed an assay that allowed us to quantitatively monitor the interaction of the C-terminal region of PC1 (cPC1) with that of PC2 (cPC2) to be able to answer the question of how Ca<sup>2+</sup> influences the PC1/PC2 complex formation. By means of the quartz crystal microbalance (QCM) technique, we were able to determine binding affinities and kinetic constants of the cPC1/cPC2 interaction using a model based on the scaled particle theory. The results suggest that cPC2 forms trimers in solution in the absence of Ca<sup>2+</sup>, which bind in a one step process to cPC1.

© 2010 Elsevier B.V. All rights reserved.

### 1. Introduction

The autosomal dominant polycystic kidney disease (ADPKD) is one of the most common monogenetic disorders that results in renal cysts development and finally leads to end stage renal disease and renal failure [1]. ADPKD occurs in 1:1000 humans as a result of a mutation in one of two genes, *pkd1* or *pkd2*. In 85% of the individuals diagnosed with ADPKD *pkd1* is mutated, while in 5–15% of the cases it is *pkd2* [2]. *pkd1* and *pkd2* encode for the proteins polycystin-1 (PC1) and polycystin-2 (PC2). PC1 is a 462 kDa integral membrane protein composed of 11 transmembrane-spanning regions, with a large extracellular N-terminus, and a smaller intracellular C-terminal part. As PC1 is located in the plasma membrane, its extracellular N-terminal domain is capable of acting as a sensor unit for fluid shear stress and it is thus very likely that PC1 plays a role in cell proliferation and differentiation [3,4]. PC2 is composed of 968 amino acids (~110 kDa) with both, the C- and N-terminus located inside the cell. With six membrane spanning regions, PC2 can be classified as a member of the transient receptor potential (TRP) channels (TRPP2) [5]. Its C-terminus harbors an EF-hand motif (Ala<sup>711</sup>-Pro<sup>797</sup>) as a potential Ca<sup>2+</sup> binding site as well as a retention signal for the endoplasmic reticulum (ER) (Asp<sup>790</sup>-Ser<sup>820</sup>) [6]. Although it has been shown that PC2 is located in the plasma membrane in certain cell lines, it is more

commonly found at the ER acting as a Ca<sup>2+</sup> permeable, non-selective cation channel [7,8]. Both, PC1 and PC2 are supposed to have a C-terminal coiled-coil domain, which are discussed to mediate the formation of a heteromeric protein–protein complex [9,10].

As PC2 and PC1 are only colocalized in the plasma membrane of certain cell lines, i.e. the primary cilium of kidney cells, the physiological role of the heteromeric protein–protein complex formation has been discussed intensively. The primary cilium could act as an antenna and gets bent due to fluid movement in the extracellular space as suggested by Nauli et al. [4]. This mechanical stress is sensed by PC1, which transmits the signal from the extracellular space to the cytosol by forming a protein–protein complex with PC2. Owing to the proposed conformational change of PC2, a Ca<sup>2+</sup>-influx is induced that activates the intracellular ryanodine receptor leading to an increase of intracellular Ca<sup>2+</sup> concentration. This signal transduction cascade is presumably responsible for tissue morphology, cell proliferation and differentiation.

Besides this activation caused by fluid shear stress, a regulation mediated by cell surface receptor stimulation as well as cell adhesion activated regulation has been proposed [9]. By electrophysiological studies on Chinese hamster ovary cells containing *pkd1* and *pkd2* genes, Hanaoka et al. [11] found that only a co-assembly of PC1 and PC2 produces a cation channel. Cai et al. [12] discovered that the channel activity depends on the cytoplasmic Ca<sup>2+</sup> concentration and can be modulated by Ser<sup>812</sup> phosphorylation. In a recent study by Schumann et al. [13], the role of Ca<sup>2+</sup> to induce conformational

\* Corresponding author. Tel.: +49 551 39 3294; fax: +49 551 39 3228.  
E-mail address: [csteine@gwdg.de](mailto:csteine@gwdg.de) (C. Steinem).

changes in a C-terminus of PC2 (cPC2) has been elucidated in detail. By means of circular dichroism-, fluorescence-, and NMR spectroscopy, they were able to identify two  $\text{Ca}^{2+}$  binding sites with different affinities ( $K_{D1} = 55 \mu\text{M}$ ,  $K_{D2} = 179 \mu\text{M}$ ). Moreover, they suggested a  $\text{Ca}^{2+}$ -dependent homodimerization of cPC2. In the absence of  $\text{Ca}^{2+}$ , cPC2 putatively forms a homodimer, while in the presence of  $\text{Ca}^{2+}$  it exists as a monomer. Yu et al. [14] however, reported that cPC2 forms a trimer, both in solution and crystal structure. Pull-down experiments with cPC2 mutants demonstrated that only the full length, trimer forming fragment (Gly<sup>833</sup>–Gly<sup>895</sup>) is capable of interacting with the C-terminal coiled-coil domain of PC1 (cPC1) [14]. The protein–protein complex was composed of three cPC2 molecules and one cPC1 domain. These findings suggest that  $\text{Ca}^{2+}$  is capable of modulating the complex formation of cPC1 with cPC2.

To investigate the protein–protein complex formation, we aimed to establish an assay that allows us to quantitatively monitor the interaction of cPC1 with cPC2 in a time resolved and label-free manner. The assay should allow us to answer questions of how  $\text{Ca}^{2+}$  influences the PC1/PC2 complex formation. The idea was to mimic the natural environment of the C-terminal part of PC1 by attaching cPC1 to a lipid bilayer. To achieve this goal, we used solid supported membranes and immobilized cPC1 via its histidine tag to a  $\text{Ni}^{2+}$  nitrilotriacetic acid (NTA-Ni) modified lipid. By means of the quartz crystal microbalance (QCM) technique we were able to investigate the binding of cPC2 without attaching any label in a time resolved manner. From the obtained results, we managed to extract binding affinities and kinetic parameters applying the scaled particle theory [15] as a function of the  $\text{Ca}^{2+}$ -concentration.

The QCM technique has proven to be a powerful tool to observe adsorption processes at solid–liquid interfaces in a label-free and time resolved manner [16,17]. Owing to the fact that the frequency response of the quartz crystal is directly proportional to the adsorbed mass at the solid–liquid interface, the QCM technique allows to study binding processes such as protein–membrane interactions, protein–protein interactions or cell and liposome adhesion [16,18–22]. Additionally, viscoelastic changes during the binding process can be monitored, which gives a closer insight into the nature of the adhered biomaterial [23,24].

## 2. Materials and methods

### 2.1. Materials

1,2-Dioleoyl-*sn*-glycero-3-phosphocholine (DOPC) and the  $\text{Ni}^{2+}$ -salt of 1,2-dioleoyl-*sn*-glycero-3-[(*N*-(5-amino-1-carboxypentyl)imidodiacetic acid)succinyl] (DOGS-NTA-Ni) were purchased from Avanti Polar Lipids (Alabaster, AL, USA). Octanethiol was obtained from Sigma-Aldrich (Steinheim, Germany). Gold (99.99%) used for the working electrodes was from Allgemeine Gold- und Silberscheideanstalt AG (Pforzheim, Germany), chromium (99.95%) was purchased from Bal TEC (Balzer, Liechtenstein). The 5 MHz AT-cut quartz crystals were obtained from KVG (Neckarbischofsheim, Germany). Water was first purified by a Millipore water purification system MilliQ RO 10 Plus and afterwards by the Millipore ultrapure water system MilliQ Plus 185 (specific resistance = 18 M $\Omega$ /cm) (Billerica, MA, USA).

### 2.2. Protein expression and purification

The C-terminal fragment of polycystin-2 (cPC2, Gly<sup>679</sup>–Val<sup>968</sup>) was expressed in *E. coli* (Rosetta strain) containing the expression vector pMAL-c2/TEV-*pkd2c*. Cells were grown to an  $\text{OD}_{595} = 0.5$  at 37 °C. Gene expression was induced by adding isopropyl- $\beta$ -D-thiogalactopyranoside to a final concentration of 1 mM. After 4 h, the cells were harvested and resuspended in lysis buffer (200 mM NaCl, 20 mM TRIS/HCl, 1 mM EDTA, pH 7.4). Subsequently, the cells were lysed by sonication and the lysates were centrifuged for 45 min at 4 °C (3100  $\times$  g). The supernatant was applied to an amylose agarose column (New England Biolabs,

Frankfurt, Germany), and the column was washed with 15 column volumes of lysis buffer. The fusion protein MBP/cPC2 (MBP = maltose binding protein) was eluted with lysis buffer containing 10 mM maltose. Cleavage of MBP/cPC2 was achieved using TEV-protease (1:100, w/w) in the presence of dithiothreitol (1:50, v/v) and EDTA (1:50, v/v). After 24 h at room temperature, the cleaved protein was dialysed against storage buffer (500 mM NaCl, 20 mM TRIS/HCl, pH 8) and purified using a NTA-Ni column. The column was first washed with 15 column volumes of storage buffer and then cPC2 was eluted with storage buffer containing 30 mM imidazole. cPC2 concentration was determined by UV/Vis-absorption using an extinction coefficient of  $\epsilon_{280} = 11,460 \text{ M}^{-1} \text{ cm}^{-1}$ .

The C-terminal fragment of polycystin-1 (cPC1, Ser<sup>4192</sup>–Thr<sup>4303</sup> with a N-terminal His-tag) was expressed in *E. coli* (strain BL21(DE3), expression vector pET21b/*pkd1c*). Induction of protein expression and cell lysis was performed as described above. cPC1 was purified using a NTA-Ni column. After washing the column with 15 column volumes of storage buffer, cPC1 was eluted with storage buffer containing 1 M imidazole. The concentration of cPC1 was determined by a Bradford assay.

histidine-tagged ezrin was expressed and purified according to a procedure described previously [25].

### 2.3. Vesicle preparation

Mixed lipid films composed of DOPC/DOGS-NTA-Ni (9:1) were prepared from stock solutions of the lipids in chloroform. Removing the chloroform under a stream of nitrogen at 32 °C and drying at 32 °C for 4 h under vacuum yields multilamellar lipid films, which were stored at 4 °C. Multilamellar vesicles (MLVs) were prepared by first swelling the mixed lipid film in the appropriate buffer (either 20 mM HEPES, 150 mM NaCl, 1 mM  $\text{CaCl}_2$ , pH 7.4 or 20 mM  $\text{KH}_2\text{PO}_4/\text{K}_2\text{HPO}_4$ , 150 mM NaCl, 1 mM EDTA, pH 7.4) followed by periodically vortexing them 3 times for 30 s every 5 min. Large unilamellar vesicles (LUVs) were obtained using the extrusion method. The MLV suspension was pressed 31 times through a polycarbonate membrane (100 nm nominal pore diameter) using a minixtruder (Liposofast, Avestin, Ottawa, Canada). The final lipid concentration was 0.2 mg/mL.

### 2.4. Preparation of lipid bilayers on gold

Gold with a thickness of 100 nm was evaporated on a 5 MHz AT-cut quartz crystal (14 mm diameter, 0.33 mm thickness) at  $5 \cdot 10^{-6}$  bar using an MED020 evaporation unit (Bal TEC GmbH, Witten, Germany). A 5 nm thin layer of chromium was used as an adhesive for the gold. To prepare a lipid bilayer on the gold electrode (0.25 cm<sup>2</sup> surface area), the quartz crystal was first cleaned in an argon plasma for 5 min (Plasma Cleaner, Harrick, NY, USA) and then placed into a Teflon chamber used for the QCM experiments. The quartz surface was immersed in a 10 mM ethanolic octanethiol (OT) solution for 2 h at room temperature. After rinsing with ethanol (5 times) and buffer (5 times), the formation of the self assembled monolayer (SAM) was controlled by impedance spectroscopy (SI 1260, Solartron Instruments, Farnborough, UK). Chemisorption of OT on the gold surface was called successful, if the specific capacitance of the monolayer was  $(2.2 \pm 0.2) \mu\text{F}/\text{cm}^2$ .

A solid supported bilayer was formed by incubating the OT monolayer with a solution of 0.2 mg/mL LUVs composed of DOPC/DOGS-NTA-Ni (9:1) for 1.5 h at room temperature. Subsequent rinsing with buffer (10 times) removed remaining vesicles. The quality of the solid supported bilayer was again controlled by means of impedance spectroscopy. The formation of a lipid monolayer atop the OT-monolayer resulted in a specific capacitance of  $(1.1 \pm 0.2) \mu\text{F}/\text{cm}^2$ .

### 2.5. QCM measurements

QCM measurements were performed using the amplitude controlled QCM200 (Stanford Research Systems, CA, USA), which allows to observe

the change in resonance frequency  $\Delta f$  due to mass adsorption as well as the change in the dynamic resistance  $\Delta R$  as a result of changes of the viscoelastic properties. The experimental set-up of the QCM is shown in Fig. 1A. The AT-cut quartz crystal was mounted in a flow through cell made of Teflon with one crystal side exposed to the liquid environment. The gold electrode of the other side of the quartz plate was connected with the oscillator circuit. The Teflon chamber was equipped with an inlet and an outlet, which allows the flow-through of buffer and protein solution under the condition of stagnation point flow geometry. Via a peristaltic pump the solutions were pumped with a constant flow rate of 0.4 mL/min. By the amplitude controlled QCM200, connected to a personal computer, the frequency change and the change in dynamic resistance was recorded. The entire system was placed in a water-jacketed Faraday cage tempered at 20 °C.

## 2.6. Kinetic modeling of the data

Reversible adsorption kinetics of small particles such as proteins on a homogenous surface can be generally described by the Langmuir model (Eq. (1)):

$$\frac{d\theta}{dt} = k_{\text{on}}\pi a^2\rho_{\infty}(1-\theta) - k_{\text{off}}\theta, \quad (1)$$

with  $k_{\text{on}}$  and  $k_{\text{off}}$  being the rate constants of particle adsorption and desorption, respectively.  $a$  is the particle radius,  $\theta$  the surface coverage, and  $\rho_{\infty}$  is the density of the particles in bulk solution.

The model is based on the assumption that particle adsorption occurs non-cooperatively on a homogeneous surface in a monomolecular fashion, where all individual binding sites have the same adsorption energy for the adsorbate. However, this model misses certain aspects of a realistic protein adsorption on a surface. First, the protein area covering one binding site can expand over more than one lattice space, which needs to be taken into account by assuming an appropriate available surface function  $\Phi(\theta)$ .  $\Phi(\theta)$  describes the available surface for deposition of particles from bulk solution as a function of coverage. For the classical Langmuir kinetics  $\Phi(\theta) = 1 - \theta$ . Second, the density of the particles in bulk solution  $\rho_{\infty}$  is different from the particle density near the surface  $\rho(\delta)$ . The flux  $j$  of the particles to the surface, given by Eq. (2), with the transport rate constant  $k_{\text{tr}}$ , accounts for the transport of the particles to the surface:

$$\frac{d\theta}{dt} = j = k_{\text{tr}}(\rho_{\infty} - \rho(\delta)). \quad (2)$$

These two refinements lead to the generalized Langmuir-equation (Eq. (3)):

$$\frac{d\theta}{dt} = k_{\text{on}}\pi a^2\rho(\delta)\Phi(\theta) - k_{\text{off}}\theta. \quad (3)$$

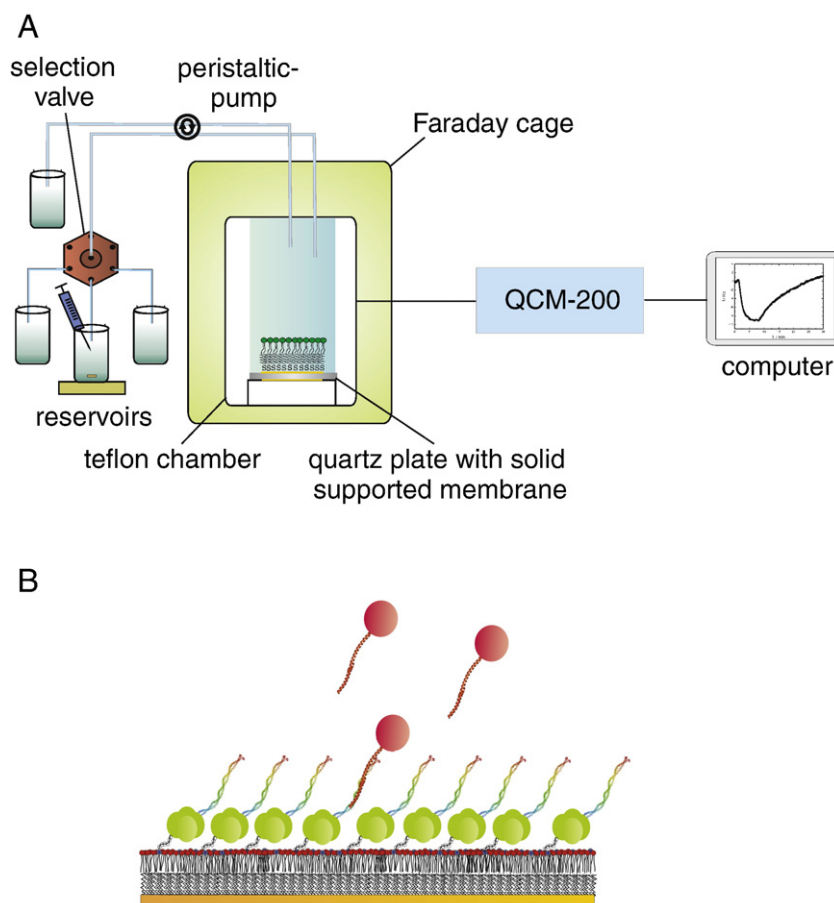


**Fig. 1.** A. Experimental setup of the quartz crystal microbalance. The quartz is mounted in a flow through cell, which is placed in a water-jacketed Faraday cage tempered at 20 °C. The protein solution is injected into a small reservoir and added to the quartz crystal via a peristaltic pump. The time resolved change in resonance frequency and dynamic resistance is read out by the QCM200 and displayed by a personal computer. B. Schematic drawing of the binding assay. cPC1 is immobilized on a solid supported membrane composed of octanethiol-DOPC/DOGS-NTA-Ni, 9:1 via its histidine tag. The solid supported membrane is prepared on a gold electrode of a 5 MHz quartz crystal. cPC2 is added in solution and binding is monitored by changes in the resonance frequency of the quartz plate.

Combining Eqs. (2) and (3) gives Eq. (4):

$$\frac{d\theta}{dt} = \frac{k_{\text{on}}\pi a^2\rho_{\infty}\Phi(\theta) - k_{\text{off}}\theta}{1 + \frac{k_{\text{on}}}{k_{\text{tr}}}\Phi(\theta)} \quad (4)$$

As the available surface function  $\Phi(\theta)$  cannot be given in a compact analytical expression, there are different strategies (i.e. developing in a virial series) that can be pursued. The scaled particle theory (SPT) is an approach to calculate the available surface function, which provides accurate results even at high coverage (Eq. (5)):

$$\Phi(\theta) = (1-\theta) \exp \left[ -3 \frac{\theta}{1-\theta} - \left( \frac{\theta}{1-\theta} \right)^2 \right] \quad (5)$$

SPT approximates the work of cavity formation in a hard-sphere fluid, which might be a submonolayer of spheres covering a surface, exactly for cavities smaller than a solvent particle. Reiss et al. [15] developed an interpolation based on a number of exact conditions imposed by geometry and thermodynamics that spans from small cavity radii to the limit of macroscopic size providing an equation of state. It has been shown that this approach correlates with data derived from dynamic Monte Carlo simulations up to a surface coverage near jamming limit [26,27].

For kinetic fitting using Eq. (4) we developed a Matlab routine based on a downhill simplex method (Nelder-Mead algorithm) combined with a built in Dormand-Prince solver (ODE 45) to integrate Eq. (4).

### 3. Results

#### 3.1. Immobilization of cPC1 on a solid-supported membrane

To investigate the interaction of cPC1 and cPC2, we first aimed to establish an immobilization strategy for cPC1 on the surface of the gold electrode of a quartz plate, which provides a natural environment for cPC1 mimicking the situation in the living cell including that the lateral mobility of the protein on the surface is guaranteed. Following this idea, we made use of solid supported membranes composed of DOPC doped with 10 mol% DOGS-NTA-Ni. The high content of DOGS-NTA-Ni ensures an almost irreversible binding of cPC1 to the chelator lipid via its histidine tag (Fig. 1B) as well as full coverage of the membrane with cPC1. This strategy is advantageous over a covalent attachment of the protein to the surface, where the protein is completely laterally immobile.

We followed the success of immobilization by the QCM technique. cPC1 was added to the DOPC/DOGS-NTA-Ni membranes in both,  $\text{Ca}^{2+}$ -free and  $\text{Ca}^{2+}$ -containing buffer with increasing concentrations. The change in resonance frequency of the 5 MHz quartz crystal was monitored until the resonance frequency did not further change upon protein addition indicating full coverage of the binding sites (Fig. 2), which prevents non-specific binding of cPC2. Rinsing with buffer results in only very little desorption of protein showing the almost fully irreversible attachment of cPC1 to the membrane. In  $\text{Ca}^{2+}$ -free buffer (150 mM NaCl, 20 mM  $\text{KH}_2\text{PO}_4/\text{K}_2\text{HPO}_4$ , 0.1 mM EDTA, pH 7.4) saturation of the binding sites was achieved at a cPC1 concentration of  $(1.1 \pm 0.5) \mu\text{M}$  resulting in an average decrease in resonance frequency of  $-\Delta f_e = (29 \pm 5) \text{ Hz}$  ( $n=8$ ). In the  $\text{Ca}^{2+}$ -containing buffer (150 mM NaCl, 20 mM HEPES, 1 mM  $\text{CaCl}_2$ , pH 7.4) a mean final concentration of cPC1 of  $(0.8 \pm 0.2) \mu\text{M}$  was required, which produced an average shift in resonance frequency of  $-\Delta f_e = (37 \pm 5) \text{ Hz}$  ( $n=5$ ). Simultaneously, for both buffer systems, a small change in the dynamic resistance  $\Delta R$  was monitored demonstrating a slight viscoelastic contribution of cPC1 upon binding (in  $\text{Ca}^{2+}$ -free buffer:  $\Delta R = (7.9 \pm 0.6) \Omega$ , in  $\text{Ca}^{2+}$ -containing buffer:  $\Delta R = (5.1 \pm 1.1) \Omega$ ).

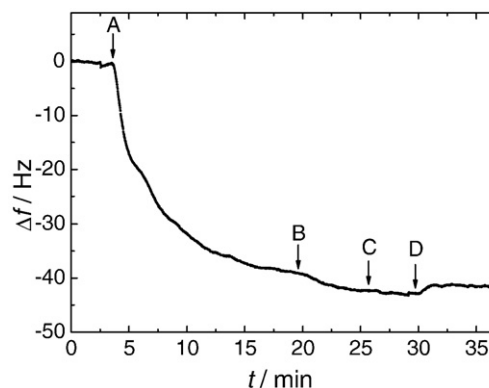


Fig. 2. Time course of the frequency shift of a 5 MHz quartz plate functionalized with a solid supported membrane (octanethiol-DOPC/DOGS-NTA-Ni, 9:1) after addition of 0.87  $\mu\text{M}$  (A), 0.98  $\mu\text{M}$  (B), 1.02  $\mu\text{M}$  (C) cPC1 in  $\text{Ca}^{2+}$  containing buffer. (D) indicates the time point of rinsing with buffer.

#### 3.2. Interaction of cPC2 with cPC1 immobilized on a solid supported membrane

Prior to the investigation of the cPC2/cPC1 interaction, control experiments were performed to rule out any non-specific binding of cPC2. As a control, the protein ezrin harboring a histidine tag, was immobilized on the DOPC/DOGS-NTA-Ni (9:1) membrane. This protein does not specifically interact with cPC2. After immobilization of ezrin, which was followed by QCM, different concentrations of cPC2 were added up to 0.4  $\mu\text{M}$  ( $\text{Ca}^{2+}$ -free buffer), and 0.2  $\mu\text{M}$  ( $\text{Ca}^{2+}$ -containing buffer). No significant change in resonance frequency was monitored independent of the chosen buffer demonstrating that non-specific binding of cPC2 to a protein decorated membrane can be excluded.

The specific interaction of cPC2 with cPC1 was also followed by QCM after immobilization of cPC1 on the DOPC/DOGS-NTA-Ni membrane. cPC2 was added to the system, which results in an immediate decrease in resonance frequency. An addition of 0.34  $\mu\text{M}$  cPC2 in 150 mM NaCl, 20 mM  $\text{KH}_2\text{PO}_4/\text{K}_2\text{HPO}_4$ , 0.1 mM EDTA, pH 7.4 results in an immediate decrease in  $\Delta f$  indicating the specific binding of cPC2 to cPC1 immobilized on the lipid membrane (Fig. 3). A change in the dynamic resistance of  $\Delta R = 1.3 \Omega$  after protein addition was detected, characteristic for an almost negligible contribution of viscoelastic effects upon binding. After a constant frequency shift of  $\Delta f_e = -8.5 \text{ Hz}$  was reached, the system was rinsed with buffer. An instant increase in resonance frequency to a value of  $\Delta f_e = 0.5 \text{ Hz}$  demonstrates that the binding of cPC1 to cPC2 is fully reversible.

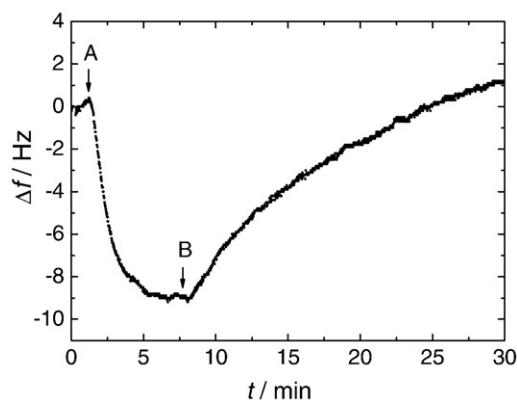


Fig. 3. Representative time course of the frequency shift upon addition of 0.34  $\mu\text{M}$  cPC2 (A) to a solid-supported membrane (octanethiol-DOPC/DOGS-NTA-Ni, 9:1) with bound cPC1. (B) indicates the time point of rinsing with  $\text{Ca}^{2+}$ -free buffer (150 mM NaCl, 20 mM  $\text{KH}_2\text{PO}_4/\text{K}_2\text{HPO}_4$ , 0.1 mM EDTA, pH 7.4).

Reversibility of the interaction of cPC2 with cPC1 was found under both conditions, in the presence and absence of  $\text{Ca}^{2+}$ .

### 3.3. Binding affinity of the cPC1/cPC2 interaction in the absence and presence of $\text{Ca}^{2+}$

To quantify the interaction of cPC1 with cPC2 as a function of  $\text{Ca}^{2+}$ , the concentration dependent change in resonance frequency  $\Delta f_e$  upon addition of cPC2 to a cPC1 covered lipid bilayer was monitored by means of QCM. The  $\Delta f_e$  values were plotted versus the monomeric cPC2 concentration in solution and the parameters of the adsorption isotherm based on the scaled particle theory (SPT) were fitted to the data (Eq. (6)) assuming the radius of cPC2 to be  $a = 1.7$  nm [13]:

$$c_{\text{cPC2}} = \frac{K_D \theta}{1 - \theta} \exp \left[ 3 \frac{\theta}{1 - \theta} + \left( \frac{\theta}{1 - \theta} \right)^2 \right] \quad (6)$$

with  $\theta = \frac{\Delta f_e}{\Delta f_{\text{max}}}$ .  $K_D$  is the dissociation constant of the cPC1/cPC2 interaction. In  $\text{Ca}^{2+}$ -free buffer (150 mM NaCl, 20 mM  $\text{KH}_2\text{PO}_4/\text{K}_2\text{HPO}_4$ , 0.1 mM EDTA, pH 7.4)  $K_D$  was determined to be  $(260 \pm 45)$  nM with a maximal resonance frequency shift of  $\Delta f_{\text{max}} = (35 \pm 5)$  Hz (Fig. 4A). However, in  $\text{Ca}^{2+}$  containing buffer (150 mM NaCl, 20 mM HEPES, 1 mM  $\text{CaCl}_2$ , pH 7.4) the binding constant of cPC2 to cPC1 was about three times larger exhibiting a dissociation constant of  $K_D = (81 \pm 30)$  nM, while the maximum shift in resonance frequency remains nearly the same ( $\Delta f_{\text{max}} = (37 \pm 5)$  Hz, Fig. 4B).

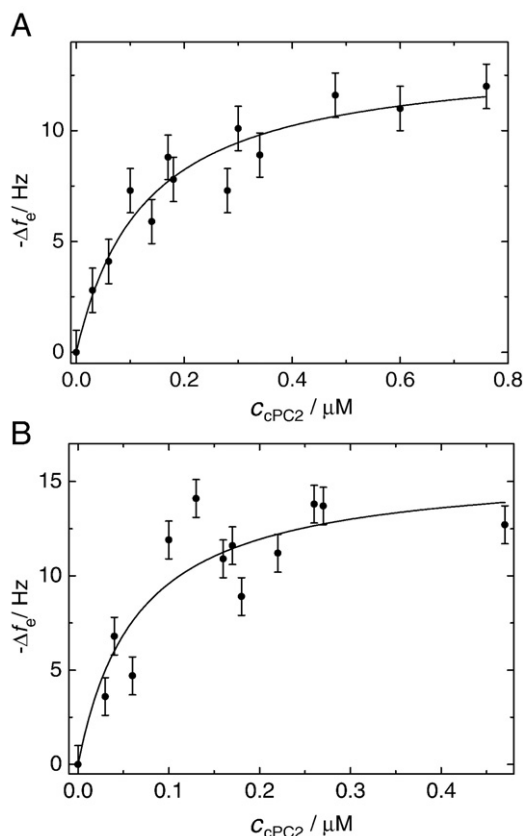


**Fig. 4.** A. Adsorption isotherm of the cPC2/cPC1 interaction in  $\text{Ca}^{2+}$ -free buffer (150 mM NaCl, 20 mM  $\text{KH}_2\text{PO}_4/\text{K}_2\text{HPO}_4$ , 0.1 mM EDTA, pH 7.4). The parameters of the adsorption isotherm (Eq. (6)) were fitted to the resonance frequency shifts obtained from the QCM data. A dissociation constant of  $(260 \pm 45)$  nM was determined for the cPC2/cPC1 complex with a maximal shift in resonance frequency of  $\Delta f_{\text{max}} = (35 \pm 5)$  Hz. B. Adsorption isotherm of the cPC2/cPC1 interaction in  $\text{Ca}^{2+}$  containing buffer (150 mM NaCl, 20 mM HEPES, 1 mM  $\text{CaCl}_2$ , pH 7.4). A dissociation constant of  $(81 \pm 30)$  nM for the cPC2/cPC1 complex was found with a maximal shift in resonance frequency of  $\Delta f_{\text{max}} = (37 \pm 5)$  Hz.

### 3.4. Kinetics of the cPC1/cPC2 interaction in the absence and presence of $\text{Ca}^{2+}$

Besides the binding affinities, we asked the question, how the binding kinetics change as a function of the  $\text{Ca}^{2+}$ -concentration. Thus, the rate constants of adsorption and desorption  $k_{\text{on}}$  and  $k_{\text{off}}$ , respectively were extracted from the time resolved changes in resonance frequency using the known  $K_D$  values according to Eq. (7):

$$K_D = \frac{k_{\text{off}}}{k_{\text{on}}} \quad (7)$$

A representative result of the fitting routine to a plot of  $\Delta f(t)$  obtained after the addition of  $0.34 \mu\text{M}$  cPC2 to a membrane coated with cPC1 is depicted in Fig. 5. The rate constants of adsorption and desorption in the absence of  $\text{Ca}^{2+}$  were determined to be  $k_{\text{on}} = (2.5 \pm 0.7) \cdot 10^4 \text{ M}^{-1} \text{ s}^{-1}$ , and  $k_{\text{off}} = (6.4 \pm 1.7) \cdot 10^{-3} \text{ s}^{-1}$ , while the transport rate constant reads  $k_{\text{tr}} = (4.4 \pm 2.7) \cdot 10^4 \text{ M}^{-1} \text{ s}^{-1}$  ( $n = 6$ ) (Table 1).

The rate constants of adsorption and desorption in the presence of  $\text{Ca}^{2+}$  were determined in the same manner resulting in  $k_{\text{on}} = (2.1 \pm 0.5) \cdot 10^4 \text{ M}^{-1} \text{ s}^{-1}$  and  $k_{\text{off}} = (1.7 \pm 0.4) \cdot 10^{-3} \text{ s}^{-1}$  ( $n = 3$ ). The transport rate constant could be determined to  $k_{\text{tr}} = (2.7 \pm 1.3) \cdot 10^4 \text{ M}^{-1} \text{ s}^{-1}$  ( $n = 2$ ) (Table 1). These results demonstrate that  $k_{\text{on}}$  is independent of the  $\text{Ca}^{2+}$ -concentration, while the desorption process is 3–4 times faster in a  $\text{Ca}^{2+}$  free solution.

## 4. Discussion

By means of the quartz crystal microbalance technique, we were able to show that cPC2 specifically interacts with cPC1 with high affinity in the absence as well as in the presence of  $\text{Ca}^{2+}$ . Using a model based on the scaled particle theory, binding constants were determined resulting in  $K_D(\text{Ca}^{2+}) = (81 \pm 30)$  nM and  $K_D(\text{EDTA}) = (260 \pm 45)$  nM. As these dissociation constants indicate the specificity of the binding, it is worth discussing the protein domains that might be involved in this interaction. It has been shown that the interaction between PC1 and PC2 is mediated through their C-termini and includes amino acid residues 822–895 of human PC2 [15]. It has further been suggested that coiled coil domains in the C-terminus of both, PC2 and PC1 are involved in the interaction. By means of a yeast two-hybrid system Qjan et al. [10] demonstrated that cPC2 interacts with cPC1 and with itself. They predicated a coiled-coil domain of PC1 between residues 4214–4248 and one in PC2 between residues

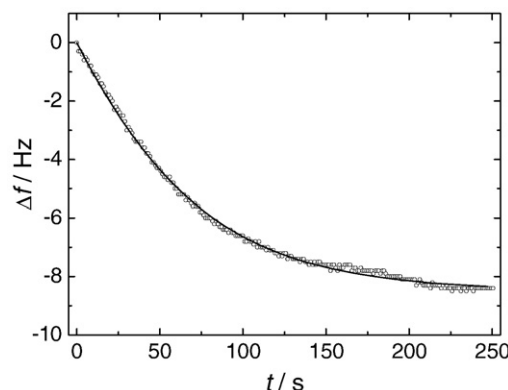


**Fig. 5.** Time dependent frequency shift after the addition of  $0.34 \mu\text{M}$  cPC2 in  $\text{Ca}^{2+}$ -free buffer (150 mM NaCl, 20 mM  $\text{KH}_2\text{PO}_4/\text{K}_2\text{HPO}_4$ , 0.1 mM EDTA, pH 7.4). The adsorption rate constant  $k_{\text{on}}$  was fitted to the data based on the SPT model taking the mass transport to the surface into account ( $k_{\text{tr}} = (4.4 \pm 2.7) \cdot 10^4 \text{ M}^{-1} \text{ s}^{-1}$  ( $n = 6$ )).  $k_{\text{on}}$  was determined to be  $(2.5 \pm 0.7) \cdot 10^4 \text{ M}^{-1} \text{ s}^{-1}$  ( $n = 6$ ). From the obtained dissociation constant  $K_D = (260 \pm 45)$  nM the rate constant of dissociation  $k_{\text{off}} = (6.4 \pm 1.8) \cdot 10^{-3} \text{ s}^{-1}$  ( $n = 6$ ) was calculated.

**Table 1**

Rate constants  $k_{\text{on}}$  and  $k_{\text{off}}$  obtained from the changes in  $\Delta f$  as a function of time in the presence and absence of  $\text{Ca}^{2+}$ . Fits to the data based on a SPT model were performed assuming a monomeric and trimeric form of cPC2 in the absence of  $\text{Ca}^{2+}$ , respectively.

|                       | $k_{\text{on}}/10^4 \text{ M}^{-1} \text{ s}^{-1}$ | $k_{\text{off}}/10^{-3} \text{ s}^{-1}$ |
|-----------------------|--|---|
| 1 mM $\text{Ca}^{2+}$ | $(2.1 \pm 0.5)$                                    | $(1.7 \pm 0.4)$                         |
| 0.1 mM EDTA (monomer) | $(2.5 \pm 0.7)$                                    | $(6.4 \pm 1.8)$                         |
| 0.1 mM EDTA (trimer)  | $(7.7 \pm 2.3)$                                    | $(6.7 \pm 2.0)$                         |

772–796 with probabilities of more than 80% using the program COILS (version 2.0) [9]. However, another program (MULTICOIL) only scores probabilities of 5.4% (all scoring dimensions included). Even though there are a few known trimeric coiled coil structures, which show a total coiled coil probability of less than 10%, the two different results highlight the ambiguity of coiled coil domain predictions [28,29]. Our results clearly demonstrate that there is a specific interaction between the C-termini of PC1 and PC2. However, whether coiled coil domains drive this interaction, remains to be elucidated.

The results we obtained were analyzed under the assumption that cPC2 is monomeric in solution, which is corroborated by the hydrodynamic radii of cPC2 found in the presence of  $\text{Ca}^{2+}$  [13]. However, Schumann et al. [13] also showed that the oligomerization state of cPC2 changes in the absence of  $\text{Ca}^{2+}$ . They determined apparent molar masses and hydrodynamic radii of cPC2 in the presence and absence of  $\text{Ca}^{2+}$  and found that the ratio of the determined apparent molar masses of cPC2 suggests a dimer or trimer in the absence of  $\text{Ca}^{2+}$ . These findings propose that the oligomerization state of cPC2 is probably a function of the  $\text{Ca}^{2+}$  concentration. With no excess of  $\text{Ca}^{2+}$ , Yu et al. [14] found a trimeric form of cPC2 in solution as well as in the crystal structure. Moreover, they demonstrated that only the trimeric form of cPC2 interacts with cPC1, while a mutant (six residues critical for the trimer formation were simultaneously mutated to Ala) that fails to form a trimer, did not interact with cPC1. It remains still an open question, whether the disturbed interaction between the cPC2 mutant and cPC1 only occurs as a result of the non-existing trimer, or whether the mutation itself affects the ability of cPC2 to interact with cPC1. Another evidence of the preferential formation of trimers of cPC2 is given by the results using the program MULTICOIL, which predicts a probability for the formation of a trimer of about 80% [29].

These results let us assume that cPC2 is trimeric in the absence of  $\text{Ca}^{2+}$  and binds as a trimer to cPC1. If we assume that only trimers

exist that bind to cPC1, the dissociation constant for this reaction would change to  $K_D(\text{EDTA}) = (87 \pm 15) \text{ nM}$ . Interestingly, in this case the affinity for both, monomeric cPC2 ( $+\text{Ca}^{2+}$ ) and trimeric cPC2 ( $-\text{Ca}^{2+}$ ) to cPC1 is almost the same. From the overall maximum frequency changes it becomes, moreover, obvious that the total coverage is the same for cPC2 bound as a monomer ( $\Delta f_{\text{max, Ca}^{2+}} = (37 \pm 5) \text{ Hz}$ ) or as the presumed trimer ( $\Delta f_{\text{max, EDTA}} = (35 \pm 5) \text{ Hz}$ ) to cPC1.

The assumption of cPC2 trimers in solution would also influence the rate constants of adsorption and desorption of the cPC1/cPC2 interaction. If a trimer is proposed, the radius of the adsorbing particle changes by a factor of 2.15, while the bulk concentration of cPC2 as well as the dissociation constant is three times smaller. The resulting rate constants obtained by fitting the SPT model to the data are given in Table 1 as a function of the  $\text{Ca}^{2+}$ -concentration. The adsorption rate constant becomes by a factor of 3.6 larger in the absence of  $\text{Ca}^{2+}$  than in its presence, while the desorption rate constant is about 4 times larger.

A conceivable scenario of the situation at the surface is depicted in Fig. 6. Binding of the cPC2 monomer to cPC1 on the membrane surface (Fig. 6A) in the presence of  $\text{Ca}^{2+}$  can occur in three independent steps with an apparent adsorption rate constant  $k_{\text{on,mono}}$ , which is the result of up to three individual rate constants  $k_{\text{on1}}$ ,  $k_{\text{on2}}$  and  $k_{\text{on3}}$ . The adsorption process of the assumed trimeric cPC2 in the absence of  $\text{Ca}^{2+}$  (Fig. 6B) would occur in one single step with a rate constant of  $k_{\text{on,trimer}} = 3.7 \cdot k_{\text{on,mono}}$ . The finding that  $k_{\text{off,trimer}} = 3.9 \cdot k_{\text{off,mono}}$  may indicate that the topologies of the cPC1/cPC2 complex are different under the given conditions or that the desorption itself again occurs in multiple steps.

As yet, the SPT model appears to be a versatile tool to evaluate the rate constants of adsorption and desorption of protein binding taking also mass transport processes into account. Mass transport limitations are a result of the large number of binding sites at the membrane provided by cPC1 [30]. Effects from mass transport can be further reduced by adding an interaction inhibitor to the system or by increasing the flow rate in the QCM experiments [30,31]. However, the flow rate of the QCM setup can only be increased within a small regime to ensure a good signal to noise ratio.

In conclusion, we were able to demonstrate that cPC2 binds to cPC1 in the absence as well as in the presence of  $\text{Ca}^{2+}$ . That the dissociation constant of the interaction of cPC1 and cPC2 in the absence of  $\text{Ca}^{2+}$  is about three times larger than in its presence suggests that cPC2 trimers exist in the absence of  $\text{Ca}^{2+}$ , which bind to cPC1.

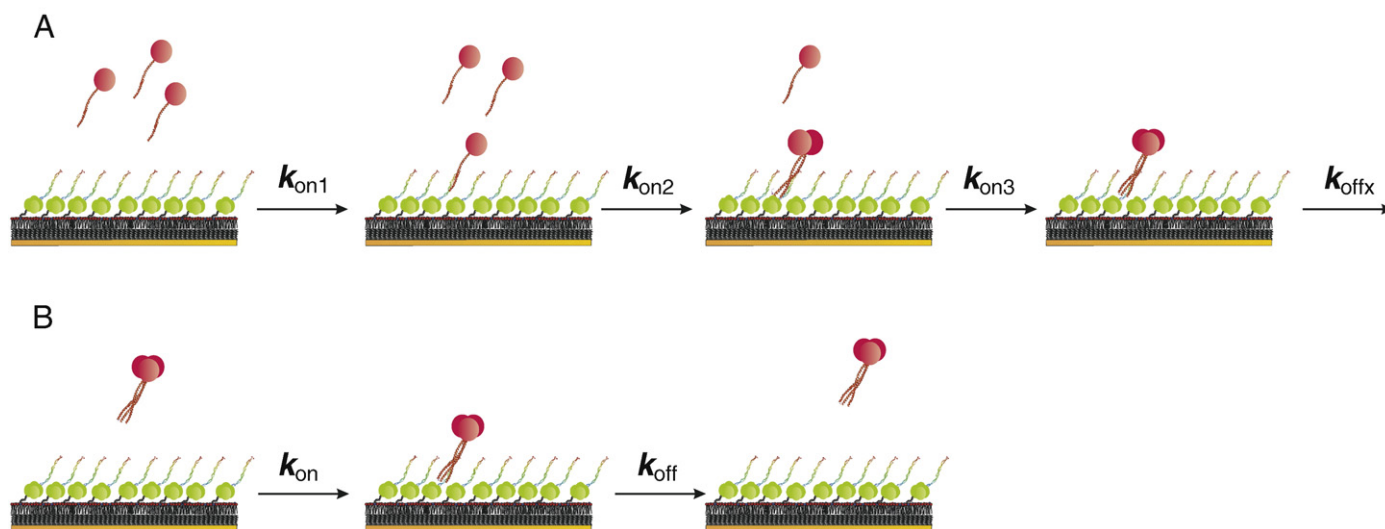


**Fig. 6.** Schematic drawing explaining the binding behavior of a cPC2 monomer to cPC1 immobilized on a solid supported membrane (A) in  $\text{Ca}^{2+}$  containing buffer. The assumed cPC2 trimer binds in a one step process (B).

## Acknowledgments

Support by Lissy Besl and Larissa Osten concerning protein purification and supply is gratefully acknowledged.

## References

- [1] P.C. Harris, V.E. Torres, Polycystic kidney disease, *Annu. Rev. Med.* 60 (2009) 321–337.
- [2] P.D. Wilson, Polycystin: new aspects of structure, function, and regulation, *J. Am. Soc. Nephrol.* 12 (2001) 834–845.
- [3] L.J. Newby, A.J. Streets, Y. Zhao, P.C. Harris, C.J. Ward, A.C. Ong, Identification, characterization, and localization of a novel kidney polycystin-1-polycystin-2 complex, *J. Biol. Chem.* 277 (2002) 20763–20773.
- [4] S.M. Nauli, F.J. Alenghat, Y. Luo, E. Williams, P. Vassilev, X. Li, A.E. Elia, W. Lu, E.M. Brown, S.J. Quinn, D.E. Ingber, J. Zhou, Polycystins 1 and 2 mediate mechanosensation in the primary cilium of kidney cells, *Nat. Genet.* 33 (2003) 129–137.
- [5] L. Birnbaumer, The TRPC class of ion channels: a critical review of their roles in slow, sustained increases in intracellular  $Ca^{2+}$  concentrations, *Annu. Rev. Pharmacol. Toxicol.* 49 (2009) 395–426.
- [6] A. Celic, E.T. Petri, B. Demeler, B.E. Ehrlich, T.J. Boggan, Domain mapping of the polycystin-2 C-terminal tail using de novo molecular modeling and biophysical analysis, *J. Biol. Chem.* 283 (2008) 28305–28312.
- [7] Y. Luo, P.M. Vassilev, X. Li, Y. Kawanabe, J. Zhou, Native polycystin 2 functions as a plasma membrane  $Ca^{2+}$ -permeable cation channel in renal epithelia, *Mol. Cell. Biol.* 23 (2003) 2600–2607.
- [8] P.M. Vassilev, L. Guo, X.Z. Chen, Y. Segal, J.B. Peng, N. Basora, H. Babakhanlou, G. Cruger, M. Kanazirska, C. Ye, E.M. Brown, M.A. Hediger, J. Zhou, Polycystin-2 is a novel cation channel implicated in defective intracellular  $Ca^{2+}$  homeostasis in polycystic kidney disease, *Biochem. Biophys. Res. Commun.* 282 (2001) 341–350.
- [9] L. Tsiokas, Function and regulation of TRPP2 at the plasma membrane, *Am. J. Physiol. Renal. Physiol.* 297 (2009) F1–F9.
- [10] F. Qian, F.J. Germino, Y. Cai, X. Zhang, S. Somlo, G.G. Germino, PKD1 interacts with PKD2 through a probable coiled-coil domain, *Nat. Genet.* 16 (1997) 179–183.
- [11] K. Hanaoka, F. Qian, A. Boletta, A.K. Bhunia, K. Piontek, L. Tsiokas, V.P. Sukhatme, W.B. Guggino, G.G. Germino, Co-assembly of polycystin-1 and -2 produces unique cation-permeable currents, *Nature* 408 (2000) 990–994.
- [12] Y. Cai, G. Anyatonwu, D. Okuhara, K.B. Lee, Z. Yu, T. Onoe, C.L. Mei, Q. Qian, L. Geng, R. Witzgall, B.E. Ehrlich, S. Somlo, Calcium dependence of polycystin-2 channel activity is modulated by phosphorylation at Ser812, *J. Biol. Chem.* 279 (2004) 19987–19995.
- [13] F. Schumann, H. Hoffmeister, R. Bader, M. Schmidt, R. Witzgall, H.R. Kalbitzer,  $Ca^{2+}$ -dependent conformational changes in a C-terminal cytosolic domain of polycystin-2, *J. Biol. Chem.* 284 (2009) 24372–24383.
- [14] Y. Yu, M.H. Ulbrich, M.H. Li, Z. Buraei, X.Z. Chen, A.C. Ong, L. Tong, E.Y. Isacoff, J. Yang, Structural and molecular basis of the assembly of the TRPP2/PKD1 complex, *Proc. Natl. Acad. Sci. U.S.A.* 106 (2009) 11558–11563.
- [15] H. Reiss, H.L. Frisch, J.L. Lebowitz, Statistical mechanics of rigid spheres, *J. Chem. Phys.* 31 (1959) 369–380.
- [16] A. Janshoff, H.-J. Galla, C. Steinem, Piezoelectric mass-sensing devices as biosensors—an alternative to optical biosensors? *Angew. Chem. Int. Ed.* 39 (2000) 4004–4032.
- [17] C. Steinem, A. Janshoff, Piezoelectric sensors, in: O.S. Wolfbeis (Ed.), *Springer Series on Chemical Sensors and Biosensors*, Springer, 2007.
- [18] F. Höök, B. Kasemo, The QCM-D technique for probing biomacromolecular recognition reactions, in: A. Janshoff, C. Steinem (Eds.), *Piezoelectric Sensors*, Springer, 2007, pp. 425–447.
- [19] R.P. Richter, J. Lai Kee Him, B. Tessier, C. Tessier, A. Brisson, On the kinetics of adsorption and two-dimensional self-assembly of annexin A5 on supported lipid bilayers, *Biophys. J.* 89 (2005) 3372–3385.
- [20] E. Lüthgens, A. Herrig, K. Kastl, C. Steinem, B. Reiss, J. Wegener, B. Pignataro, A. Janshoff, Adhesion of liposomes: a quartz crystal microbalance study, *Meas. Sci. Technol.* 14 (2003) 1865–1875.
- [21] S. Faiß, K. Kastl, A. Janshoff, C. Steinem, Formation of irreversibly bound annexin A1 protein domains on POPC/POPS solid supported membranes, *Biochim. Biophys. Acta* 1778 (2008) 1601–1610.
- [22] A. Janshoff, C. Steinem, Label-free detection of protein-ligand interactions by the quartz crystal microbalance, in: G.U. Nienhaus (Ed.), *Protein-ligand interactions*, Humana Press, Totowa, New Jersey, 2005, pp. 47–63.
- [23] E. Tellechea, D. Johannsmann, N.F. Steinmetz, R.P. Richter, I. Reviakine, Model-independent analysis of QCM data on colloidal particle adsorption, *Langmuir* 25 (2009) 5177–5184.
- [24] P. Bingen, G. Wang, N.F. Steinmetz, M. Rodahl, R.P. Richter, Solvation effects in the quartz crystal microbalance with dissipation monitoring response to biomolecular adsorption. A phenomenological approach, *Anal. Chem.* 80 (2008) 8880–8890.
- [25] A. Herrig, M. Janke, J. Austermann, V. Gerke, A. Janshoff, C. Steinem, Cooperative adsorption of ezrin on PIP<sub>2</sub>-containing membranes, *Biochemistry* 45 (2006) 13025–13034.
- [26] E. Lüthgens, Ph.D. thesis, Johannes Gutenberg Universität, 2005.
- [27] K. Kastl, M. Menke, E. Lüthgens, S. Faiß, V. Gerke, A. Janshoff, C. Steinem, Partially reversible adsorption of annexin A1 on POPC/POPS bilayers investigated by QCM measurements, SFM, and DMC simulations, *Chem. Biochem.* 7 (2006) 106–115.
- [28] A. Lupas, Predicting coiled-coil regions in proteins, *Curr. Opin. Struct. Biol.* 7 (1997) 388–393.
- [29] E. Wolf, P.S. Kim, B. Berger, MultiCoil: a program for predicting two- and three-stranded coiled coils, *Protein. Sci.* 6 (1997) 1179–1189.
- [30] D.G. Myszka, Kinetic analysis of macromolecular interactions using surface plasmon resonance biosensors, *Curr. Opin. Biotechnol.* 8 (1997) 50–57.
- [31] D.J. O'Shannessy, D.J. Winzor, Interpretation of deviations from pseudo-first-order kinetic behavior in the characterization of ligand binding by biosensor technology, *Anal. Biochem.* 236 (1996) 275–283.